

Dynamic Phase Alignment in Inertial Alfvén Turbulence

Lucio M. Milanese* and Nuno F. Loureiro

Plasma Science and Fusion Center, Massachusetts Institute of Technology, Cambridge, MA 02139, USA

Maximilian Daschner

*Plasma Science and Fusion Center, Massachusetts Institute of Technology, Cambridge, MA 02139, USA and
ETH Zurich, CH-8093 Zürich, Switzerland*

Stanislav Boldyrev

*Department of Physics, University of Wisconsin-Madison, Madison, WI 53706, USA and
Space Science Institute, Boulder, CO 80301, USA*

(Dated: October 2, 2020)

In weakly-collisional plasma environments with sufficiently low electron beta, Alfvénic turbulence transforms into inertial Alfvénic turbulence at scales below the electron skin-depth, $k_{\perp}d_e \gtrsim 1$. We argue that, in inertial Alfvénic turbulence, both energy and generalized kinetic helicity exhibit direct cascades. We demonstrate that the two cascades are compatible due to the existence of a strong scale-dependence of the phase alignment angle between velocity and magnetic field fluctuations, with the phase alignment angle scaling as $\cos \alpha_k \propto k_{\perp}^{-1}$. The kinetic and magnetic energy spectra scale as $\propto k_{\perp}^{-5/3}$ and $\propto k_{\perp}^{-11/3}$, respectively. As a result of the dual direct cascade, the generalized-helicity spectrum scales as $\propto k_{\perp}^{-5/3}$, implying progressive balancing of the turbulence as the cascade proceeds to smaller scales in the $k_{\perp}d_e \gg 1$ range. Turbulent eddies exhibit a phase-space anisotropy $k_{\parallel} \propto k_{\perp}^{5/3}$, consistent with critically-balanced inertial Alfvén fluctuations. Our results may be applicable to a variety of geophysical, space, and astrophysical environments, including the Earth’s magnetosheath and ionosphere, solar corona, non-relativistic pair plasmas, as well as to strongly rotating non-ionized fluids.

Introduction. Many important turbulent plasma environments are characterized by a low ratio of the electron plasma pressure to magnetic energy density, that is, low β_e , in addition to weak collisionality. Examples are the ionosphere [1, 2], the Earth’s magnetosheath [3], the solar corona [4, 5] and some instances of the solar wind [6, 7]. Turbulence may play a role in structure formation, energy dissipation, magnetic reconnection, heat conduction, and other processes relevant for the dynamics and thermodynamics of such systems [6, 8–16]. Despite vigorous investigation, the nature of turbulent fluctuations in low beta regimes remains incompletely understood and continues to attract considerable interest [3, 17–20].

At scales below the electron skin depth in plasmas with sufficiently low β_e , the dominant low-frequency plasma modes are arguably nonlinear inertial Alfvén waves, whose turbulent cascade is governed by the existence of two ideal invariants: energy and generalized kinetic helicity. Turbulent dynamics in the presence of two invariants is poorly understood in both plasmas and non-ionized fluids [21, 22]. It is possible that both invariants are subject to a forward (direct) cascade, or that one of them cascades forward and the other backward [20–25]. When both quantities cascade forward, one can argue in favor of the cascade of either invariant setting the nonlinear eddy turn-over time [22], greatly complicating the analysis and leading to different predictions and understanding of the underlying turbulent dynamics.

In this Letter, we propose that, in inertial Alfvén turbulence, both energy and (kinetic) helicity cascade forward, and it is the cascade of energy, rather than that of helicity, that determines the cascade time. We demonstrate that, rather remarkably, this is achieved via a strongly scale-dependent *phase alignment* between fluctuations of electric and magnetic potentials, which manages to suppress helicity while allowing the energy cascade to proceed unhindered. Our phenomenological model predicts the spectra of magnetic, kinetic, and helicity fluctuations in the inertial kinetic regime, shown here to be in good agreement with the results of numerical simulations.

More broadly, we conjecture that the phenomenon of scale-dependent phase alignment uncovered in this work may be the mechanism underpinning the joint forward cascade of two ideal invariants in other physical systems, including nonconducting fluids described by the Navier-Stokes equation [22, 24, 26, 27].

Model equations. We consider a plasma permeated by a strong magnetic field, $B_0\hat{z}$, such that the total field is $\mathbf{B} = B_0\hat{z} + \delta\mathbf{B}_{\perp}$, with $\delta B_{\perp}/B_0 \ll 1$. The evolutionary equations that we adopt are:

$$\frac{\partial}{\partial t} \nabla_{\perp}^2 \phi + \{\phi, \nabla_{\perp}^2 \phi\} = \{\psi, \nabla_{\perp}^2 \psi\} + V_A \frac{\partial}{\partial z} \nabla_{\perp}^2 \psi + f_{\phi}, \quad (1)$$

$$\frac{\partial}{\partial t} (1 - d_e^2 \nabla_{\perp}^2) \psi + \{\phi, (1 - d_e^2 \nabla_{\perp}^2) \psi\} = V_A \frac{\partial \phi}{\partial z} + f_{\psi}. \quad (2)$$

Here, ϕ denotes the stream function, related to the $\mathbf{E} \times \mathbf{B}$ flow velocity by $\mathbf{v}_{\perp} = \hat{z} \times \nabla_{\perp} \phi$, and ψ is the flux function,

* milanese@mit.edu

related to the perpendicular component of the magnetic field by $\delta\mathbf{B}_\perp/\sqrt{4\pi\rho} = \hat{\mathbf{z}} \times \nabla_\perp \psi$, with ρ the mass density. The Poisson bracket is defined as $\{A, B\} = \partial_x A \partial_y B - \partial_x B \partial_y A$, the Alfvén speed is $V_A = B_0/\sqrt{4\pi\rho}$, and f_ϕ and f_ψ are forcing terms to be described later. The only kinetic effect included in these equations is the electron inertia, characterized by d_e , the electron skin-depth [28].

These equations describe low beta non-relativistic pair-plasmas [29], as well as electron-ion plasmas in the ‘ultralow’ beta limit, $\beta_e \sim \beta_i \ll m_e/m_i$ [30]. The modes described by these equations are (as we show below) the inertial Alfvén modes. However, quite importantly, our equations are also pertinent to a wide range of other environments. When $k_\perp^2 d_e^2 \gg 1 + 2/\beta_i$, our equations are structurally identical to Eqs. (19) and (20) of Ref. [3] which were derived under the assumptions of $\beta_i \sim 1$ and $\beta_e \ll 1$. The dominant low-frequency modes there are inertial kinetic Alfvén waves ($\omega < k_\perp v_{thi}$, with v_{thi} the ion thermal speed) [3, 31]. In addition, in the limit $k_\perp^2 d_e^2 \gg 1$, Eqs. (1-2) are structurally equivalent to Eqs. (25) and (26) of Ref. [3], which describe inertial whistler waves ($\omega > k_\perp v_{thi}$) in reduced electron MHD. One can also demonstrate that, quite remarkably, in the limit $k_\perp^2 d_e^2 \gg 1$, our equations map onto the equations describing rapidly rotating non-ionized fluids [32]. A short derivation of model Eqs. (1-2) is presented in the Supplemental Material, where a summary of their regimes of applicability is also included.

Eqs. (1-2) have two quadratic invariants: total energy,

$$\mathcal{E} = \frac{1}{2} \int dV \left\{ (\nabla_\perp \psi)^2 + d_e^2 (\nabla_\perp^2 \psi)^2 + (\nabla_\perp \phi)^2 \right\}, \quad (3)$$

and generalized kinetic helicity,

$$\mathcal{H} = \int dV \left\{ \nabla_\perp^2 \phi (1 - d_e^2 \nabla_\perp^2) \psi \right\}, \quad (4)$$

which reduces to cross-helicity at MHD scales ($k_\perp d_e \ll 1$).

The only linear mode supported by these equations is the inertial Alfvén wave, with dispersion relation and eigenfunctions given by:

$$\omega_l = \pm \frac{k_z V_A}{\sqrt{1 + k_\perp^2 d_e^2}}, \quad \phi = \pm \sqrt{1 + k_\perp^2 d_e^2} \psi. \quad (5)$$

Inertial Alfvén turbulence. The focus of our Letter is on turbulence in the kinetic range $k_\perp d_e \gg 1$. In the opposite limit of $k_\perp d_e \ll 1$, Eqs. (1-2) become the reduced MHD (RMHD) equations [33–35], and thus results obtained for RMHD are expected to apply [36]. Following Ref. [29], the energy flux at scales $k_\perp d_e > 1$ is expected to be $\varepsilon \sim k_\perp^2 \phi_\lambda^2 / \tau_\lambda$, where τ_λ is the eddy turnover time at the scale $\lambda \sim k_\perp^{-1}$, and $\tau_\lambda = 1/\omega_{nl} \sim 1/(k_\perp^2 \phi_\lambda)$. This yields $\phi_\lambda \sim \varepsilon^{1/3} k_\perp^{-4/3}$, leading to the scaling of the spectrum of perpendicular kinetic energy $\mathcal{E}_K(k_\perp) dk_\perp \sim \varepsilon^{2/3} k_\perp^{-5/3} dk_\perp$. For $k_\perp^2 d_e^2 \gg 1$, equipartition between parallel and perpendicular kinetic energies,

i.e., between the second and third terms in Eq. (3), results in $\psi_\lambda \sim k_\perp^{-7/3}$ from which follows the magnetic energy spectrum $\mathcal{E}_B(k_\perp) dk_\perp \sim \varepsilon^{2/3} k_\perp^{-11/3} dk_\perp$. Finally, postulating critical balance of the fluctuations in this range (i.e., that the characteristic linear and nonlinear frequencies of the system approximately balance at each scale [35, 37]), yields

$$k_\parallel \sim \varepsilon^{1/3} d_e V_A^{-1} k_\perp^{5/3}. \quad (6)$$

Using the above scalings for ϕ_λ and ψ_λ , we would predict the helicity spectrum to scale as $\mathcal{H}(k_\perp) dk_\perp \sim k_\perp^{-2/3} dk_\perp$ in the kinetic range. However, as discussed in Ref. [29], in this case the helicity flux cannot be constant; rather it should *increase* at small scales, leading to a contradiction. If, on the other hand, we assume that the scaling of the fields should be determined by a direct helicity cascade, we would formally conclude that the energy cannot cascade toward small scales at $k_\perp d_e > 1$. This contradiction can be solved if, as conjectured in Ref. [29], the helicity flux at scales $k_\perp d_e \gg 1$ is written as

$$(k_\perp^2 \phi_\lambda) (d_e^2 k_\perp^2 \psi_\lambda) R_\lambda / \tau_\lambda \sim \varepsilon_H, \quad (7)$$

where R_λ is a scale-dependent cancellation factor. Requiring that the flux of kinetic helicity be constant in the kinetic range and enforcing consistency between energy and helicity fluxes leads to

$$R_\lambda \sim \varepsilon_H (k_\perp^2 \phi_\lambda)^{-2} (d_e^2 k_\perp^2 \psi_\lambda)^{-1} \sim \varepsilon_H (k_\perp d_e)^{-1}. \quad (8)$$

When the cancellation factor is present, the simultaneous direct cascades of *both* energy and helicity become possible, and we arrive at a qualitatively different prediction for the helicity spectrum, $\mathcal{H}(k_\perp) dk_\perp \sim k_\perp^{-5/3} dk_\perp$. In what follows we demonstrate that the cancellation factor is a manifestation of a new phenomenon that we call “*dynamic phase alignment*”: an increasing correlation between the *phases* of the fluctuating magnetic and velocity fields as the cascade progresses towards smaller scales.

Numerical setup. We now report on direct numerical simulations carried out to test these theoretical predictions. We integrate Eqs. (1-2) with the code **Viriato** [38] on a triply periodic domain using a grid of $N_\perp^2 \times N_\parallel$ points. Hyper-dissipation terms of the form $\nu_H \nabla_\perp^6$ are included on the right-hand side of both equations, with ν_H set to remove energy at the grid scale. Energy is injected via delta-correlated forcing terms of the form

$$f_{\phi,\psi} = C_{\phi,\psi} \alpha_\pm \delta(k_x - k_{x0}) \delta(k_y - k_{y0}) \cos(k_z z), \quad (9)$$

where C_ϕ and C_ψ are randomly chosen complex numbers determining the phase of the mode being excited ($C_\phi \neq C_\psi$, and $|C_{\phi,\psi}| = 1$), and $\alpha_\pm > 0$ are numerical coefficients determining the strength of the drive, their subscript relating to positive and negative (generalized) kinetic helicity injection, as discussed below. The mode

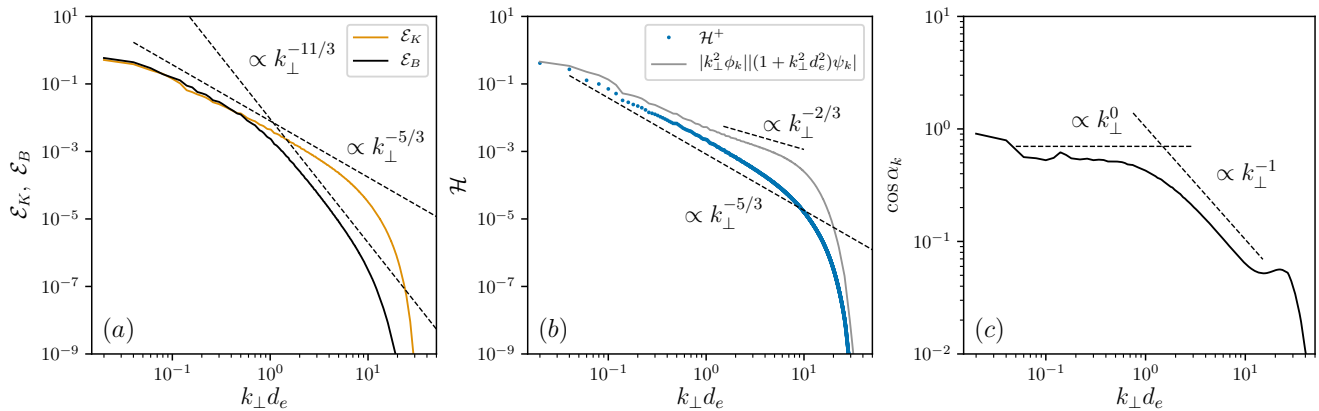


FIG. 1. Simulation A1. (a) Spectra of magnetic and kinetic energy. (b) Spectra of kinetic helicity and of the product of the absolute value of the factors in the integrand of Eq. (4). (c) Scale dependence of the average phase angle between fluctuations of electric and magnetic potential in Fourier space.

numbers k_{x0} , k_{y0} and k_{z0} are randomly chosen from a predetermined range and at every time step they are the same for both f_ϕ and f_ψ .

From Eqs. (4, 9), one can show that the kinetic helicity injected at any time step by the forcing terms is given by

$$\mathcal{H}_{inj}^\pm \propto k_{\perp 0}^2 (1 + k_{\perp 0}^2 d_e^2) \alpha_\pm^2 \text{Re}[C_\phi C_\psi], \quad (10)$$

where $k_{\perp 0}^2 = k_{x0}^2 + k_{y0}^2$. When $\text{Re}[C_\phi C_\psi] > 0$, i.e., when the phase between f_ϕ and f_ψ is such that positive helicity is injected at a particular time step, the α_+ coefficient is used in the forcing terms. When $\text{Re}[C_\phi C_\psi] < 0$, the coefficient α_- is used instead. We define the ratio of positive to negative kinetic helicity injection as $\mathcal{R}_\mathcal{H} \equiv \mathcal{H}_{inj}^+ / \mathcal{H}_{inj}^-$. The ratio of the coefficients is set as $\alpha_+ / \alpha_- = \sqrt{\mathcal{R}_\mathcal{H}}$.

Table I summarizes key parameters of the simulations performed. In all cases, energy is injected at the largest scales, where $k_\perp d_e < 1$. In runs A1 and B2 net positive kinetic helicity is injected by the forcing terms ($\mathcal{R}_\mathcal{H} = 10$ and $\mathcal{R}_\mathcal{H} = 30$, respectively), while in run B1 no net kinetic helicity is injected ($\mathcal{R}_\mathcal{H} = 1$). Run A1 aims at capturing the dynamics in both the RMHD and kinetic range, and providing insight into how the transition between the two regimes occurs. Simulations of type B aim at capturing in more detail the turbulent dynamics in the kinetic range.

| ID | N_\perp | N_\parallel | $(k_\perp d_e)_{min}$ | $\mathcal{R}_\mathcal{H}$ |
|----|-----------|---------------|-----------------------|---------------------------|
| A1 | 2048 | 2048 | 0.02 | 10 |
| B1 | 768 | 4096 | 0.3 | 1 |
| B2 | 768 | 4096 | 0.3 | 30 |

TABLE I. Summary of key simulation parameters.

Energy spectra. Figs. 1a and 1b show the energy and (generalized kinetic) helicity spectra (obtained from time-averaged data after steady state is reached) for simulation A1. The magnetic energy spectrum is seen

to smoothly transition from $\sim k_\perp^{-5/3}$ to $\sim k_\perp^{-11/3}$ at $k_\perp d_e \approx 1$, whereas the kinetic energy scales as $\sim k_\perp^{-5/3}$ throughout the inertial range, as does the helicity spectrum. These observations are in good agreement with the theoretical predictions, and offer an immediate confirmation of the existence of the scale-dependent cancellation factor $R_\lambda \sim 1/k_\perp$ at scales $k_\perp d_e > 1$.

Runs of type B confirm the kinetic range results over a larger scale range; see Figs. 2b and 2d. The energy spectra are not significantly affected by the ratio of positive to negative helicity injected in the system. When no net helicity is injected in the system, the spectrum of helicity is not well defined (Fig. 2b). One can observe that the sign of kinetic helicity is different at different perpendicular wavenumbers k_\perp in the inertial range, and its value is zero when spatially averaged over the entire simulation domain and time averaged over the steady state. When instead net helicity is injected in the system, a well-defined spectrum is observed, exhibiting a scaling $\sim k_\perp^{-5/3}$ (Fig. 2d), as in simulation A1.

To characterize eddy anisotropy, we consider that the parallel wavenumber of a fluctuating field ϕ at perpendicular scale k_\perp may be approximated as [39]

$$k_\parallel \approx \left(\frac{\langle |\mathbf{B}_0 \partial_z \phi_{k_\perp} + \delta \mathbf{B}_{k_\perp} \cdot \nabla \phi_{k_\perp}|^2 \rangle}{\langle B_{k_\perp}^2 \rangle \langle \phi_{k_\perp}^2 \rangle} \right)^{1/2}, \quad (11)$$

where $\langle \dots \rangle$ denotes spatial averaging. In the kinetic range, electromagnetic fluctuations are small because electron inertia ($k_\perp^2 d_e^2 \partial_t \psi$) dominates over the inductive part of the electric field ($\partial_t \psi$) in Eq. (2). Therefore, turbulence in this regime is essentially electrostatic, i.e., $\mathbf{B}_0 \partial_z \phi_{k_\perp} \gg \delta \mathbf{B}_{k_\perp} \cdot \nabla \phi_{k_\perp}$, and thus $k_\parallel \approx k_z$. The scatter plots in Figs. 2a and 2c show, for each value of k_z , the corresponding value of k_\perp at which the energy of the ϕ fluctuations is largest. The data exhibit the scaling $k_\parallel \propto k_\perp^{5/3}$, in agreement with Eq. (6), confirming that

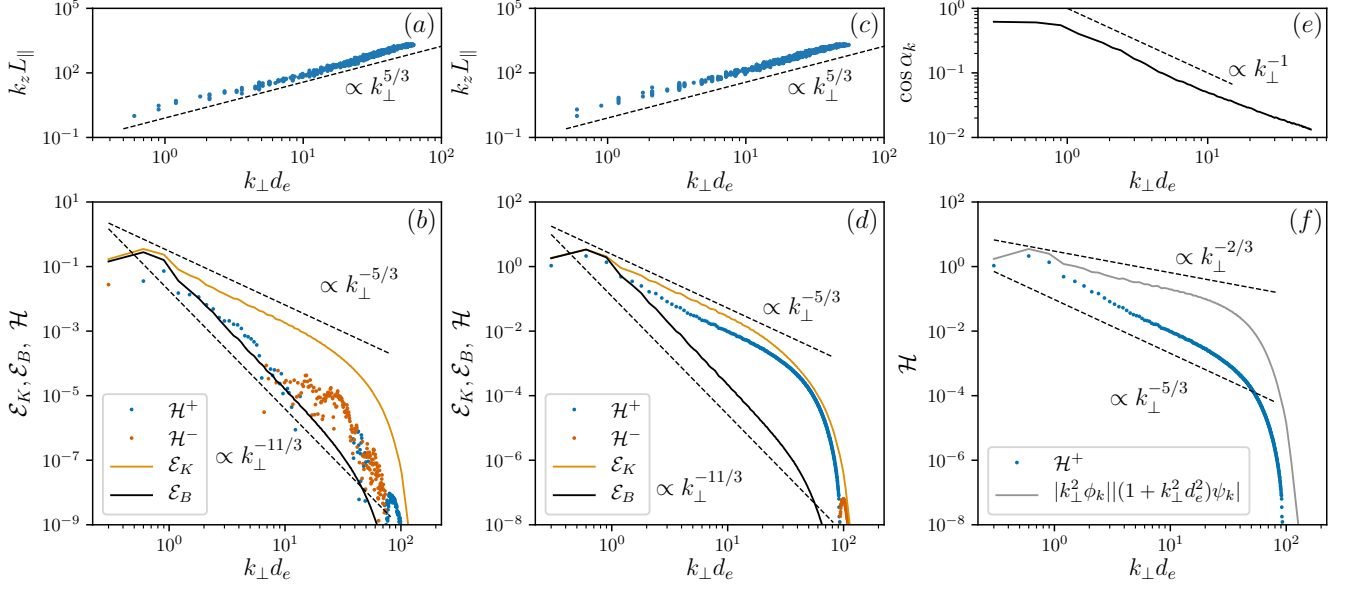


FIG. 2. Eddy anisotropy scaling for simulations B1 and B2 (subplots (a) and (c), respectively). Spectra of kinetic helicity, and of kinetic and magnetic energy for simulations B1 and B2 (subplots (b) and (d), respectively). Different colors are used to represent the presence of net positive or negative helicity in perpendicular wavenumber shells. Subplot (f) presents the spectra of kinetic helicity and of the product of the absolute value of the factors in the integrand of Eq. (4) in simulation B2. The corresponding average value of the cosine of the phase angle (Eq. (12)) as a function of scale is shown in subplot (e).

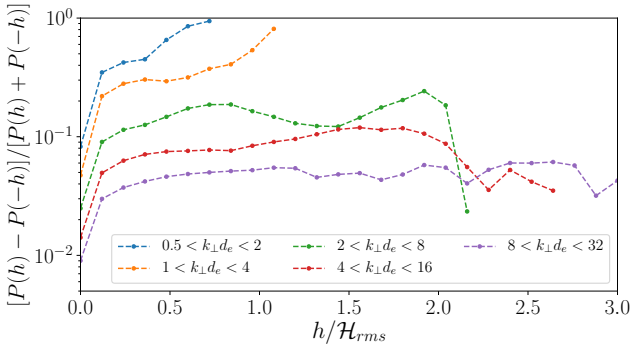


FIG. 3. Relative difference between the PDF of positive and negative helicity density obtained from band-pass filtered data from simulation B2.

the inertial Alfvén cascade is critically balanced.

Kinetic helicity spectrum and dynamic phase alignment. The net kinetic helicity at each wavenumber is a function of the absolute value of the Fourier coefficients $|\phi_k|$ and $|\psi_k|$, and of the phase angle between them, α_k . For a given k_\perp , the average value of α_k is given by

$$\cos \alpha_k = \frac{1}{2} \frac{\langle k_\perp^2 \phi_{k\perp} (1 + d_e^2 k_\perp^2) \psi_{k\perp}^* + c.c. \rangle}{\langle |k_\perp^2 \phi_{k\perp}| | (1 + d_e^2 k_\perp^2) \psi_{k\perp} | \rangle}, \quad (12)$$

where the numerator represents net kinetic helicity at a given perpendicular wavenumber. In the $k_\perp d_e < 1$ range,

the spectra of $|k_\perp^2 \phi_{k\perp}| |\psi_{k\perp}|$ and of generalized kinetic helicity (which turns into cross helicity at such scales) are both expected to exhibit the scaling of the MHD energy spectrum, and thus $\cos \alpha_k$ should not depend strongly on scale. At scales $k_\perp d_e > 1$, however, the spectrum of $|k_\perp^2 \phi_{k\perp}| |k_\perp^2 d_e^2 \psi_{k\perp}|$ is expected to scale as $k_\perp^{-2/3}$, while we predict, and observe, kinetic helicity to scale as $k_\perp^{-5/3}$. We thus expect $\cos \alpha_k \propto k_\perp^{-1}$. This is confirmed in Fig. 1c: in the RMHD range, $\cos \alpha_k$ does not vary strongly as a function of scale. After a smooth transition at $k_\perp d_e \approx 1$, the scaling of $\cos \alpha_k$ asymptotes to $\propto k_\perp^{-1}$ for $k_\perp d_e > 1$. Fig. 2e confirms the scaling $\cos \alpha_k \propto k_\perp^{-1}$ in the kinetic range.

When $\cos \alpha_k = 0$, kinetic helicity is zero and the system is in a perfectly balanced state. The scaling $\cos \alpha_k \propto k_\perp^{-1}$ therefore implies that the turbulence becomes progressively more balanced as the cascade proceeds deeper in the kinetic range. This statement is corroborated by results from simulation B2 shown in Fig. 3, in which we present the scale-dependence of asymmetries in the probability density function (PDF) of generalized kinetic helicity density (h). We plot, at different perpendicular scales, the relative difference between the PDF of positive and negative helicity density, i.e., $P(h)$ and $P(-h)$, for $h \in [0, 3 \mathcal{H}_{rms}]$, where \mathcal{H}_{rms} is the root mean square value of helicity density obtained from unfiltered data. As the selection of scales included in the band-pass filter moves towards larger values of k_\perp , the relative dif-

ference between $P(h)$ and $P(-h)$ becomes smaller, showing that the PDF is progressively more symmetric and thus more balanced (a perfectly symmetric PDF implies that the turbulence is balanced, as $\mathcal{H} = \int P(h)h dh = 0$).

Conclusions. In this Letter, we showed that, in inertial Alfvén turbulence, both energy and generalized kinetic helicity cascade forward, with the cascade of energy determining the nonlinear eddy turn-over time. Helicity is found to scale as $\mathcal{H} \propto k_{\perp}^{-5/3}$ in the kinetic range, a result that is underpinned by a scale-dependent alignment angle, $\cos \alpha_k \propto k_{\perp}^{-1}$, between the Fourier phases of magnetic and velocity fields. Consequently, turbulence becomes progressively more balanced as the cascade proceeds deeper into the kinetic range.

The results presented in this Letter may be valuable for interpreting the direct measurements of low-beta turbulence in space plasmas [4–7], as well as for other astrophysical and geophysical turbulent systems where dual energy and kinetic helicity cascades are possible (e.g., sub-relativistic pair plasma [29], whose experimental realization is upcoming [40, 41], ionospheric [1, 2] and magnetospheric plasmas [3], and strongly rotating nonconducting fluids [42]). Another context where our findings may be pertinent is Navier-Stokes (NS) turbulence. Simulations reveal a $k^{-5/3}$ scaling of kinetic helicity and a scale-dependent progressive balancing of turbulence (restoration of mirror symmetry) [24, 26, 27] whose un-

derlying dynamics is not fully understood. We conjecture that the novel mechanism of dynamic phase alignment uncovered in this work may also be at play in NS turbulence, and account for those results. While the details of the nonlinear interactions in plasma and NS turbulence are different, our conjecture is based on commonalities between particular aspects of the joint forward cascade of energy and (generalized) kinetic helicity. In particular, in both systems, a ‘naïve’ estimate of the spectral scaling of helicity, without the inclusion of a scale-dependent phase alignment factor, would yield a scaling $\sim k^{-2/3}$, which, if realized, would prevent energy from cascading forward. In both systems a scaling $\mathcal{H} \sim k^{-5/3}$ is instead observed [24, 27], which may be underpinned, in the case of NS turbulence, by a scale-dependent alignment between the phases of velocity and vorticity fluctuations.

Work supported by DoE grant No. DE-FG02-91ER54109 (L.M.M. and N.F.L.), NSF CAREER award No. 1654168 (N.F.L.), the Prof. Amar G. Bose Research Fellows Program at MIT (L.M.M. and N.F.L.), and NSF grant No. PHY-1707272, NASA grant No. 80NSSC18K0646, and DOE grant No. DESC0018266 (S.B.). This research used resources of the facilities of the Massachusetts Green High-Performance Computing Center (MGHPCC) and of the National Energy Research Scientific Computing Center (NERSC), a U.S. Department of Energy Office of Science User Facility operated under Contract No. DE-AC02-05CH11231.

-
- [1] C. K. Goertz and B. W. Boswell, Magnetosphere-Ionosphere coupling, *Journal of Geophysical Research* **84**, 7239 (1979).
- [2] A. Kumari, R. P. Sharma, and N. Yadav, Inertial Alfvén wave induced turbulent spectra in aurora, *Astrophysics and Space Science* **351**, 81 (2014).
- [3] C. H. K. Chen and S. Boldyrev, Nature of Kinetic Scale Turbulence in the Earth’s Magnetosheath, *The Astrophysical Journal* **842**, 122 (2017).
- [4] M. J. Aschwanden, A. I. Poland, and D. M. Rabin, The new solar corona, *Annual Review of Astronomy and Astrophysics* **39**, 175 (2001).
- [5] S. R. Cranmer, Coronal holes, *Living Reviews in Solar Physics* **6**, 3 (2009).
- [6] C. W. Smith, D. J. Mullan, N. F. Ness, R. M. Skoug, and J. Steinberg, Day the solar wind almost disappeared: Magnetic field fluctuations, wave refraction and dissipation, *Journal of Geophysical Research: Space Physics* **106**, 18625 (2001).
- [7] C. H. Chen, L. Leung, S. Boldyrev, B. A. Maruca, and S. D. Bale, Ion-scale spectral break of solar wind turbulence at high and low beta, *Geophysical Research Letters* **41**, 8081 (2014).
- [8] P. L. Similon and R. N. Sudan, Plasma Turbulence, *Annual Review of Fluid Mechanics* **22**, 317 (1990).
- [9] D. Biskamp, *Magnetohydrodynamic Turbulence* (Cambridge University Press, 2003).
- [10] T. D. Phan, J. P. Eastwood, M. A. Shay, J. F. Drake, B. U. Sonnerup, M. Fujimoto, P. A. Cassak, M. Øieroset, J. L. Burch, R. B. Torbert, A. C. Rager, J. C. Dorelli, D. J. Gershman, C. Pollock, P. S. Pyakurel, C. C. Haggerty, Y. Khotyaintsev, B. Lavraud, Y. Saito, M. Oka, R. E. Ergun, A. Retino, O. Le Contel, M. R. Argall, B. L. Giles, T. E. Moore, F. D. Wilder, R. J. Strangeway, C. T. Russell, P. A. Lindqvist, and W. Magnes, Electron magnetic reconnection without ion coupling in Earth’s turbulent magnetosheath, *Nature* **557**, 202 (2018).
- [11] C. Vega, V. Roytershteyn, G. L. Delzanno, and S. Boldyrev, Electron-only Reconnection in Kinetic-Alfvén Turbulence, *The Astrophysical Journal* **893**, L10 (2020).
- [12] J. E. Stawarz, J. P. Eastwood, T. D. Phan, I. L. Gingell, M. A. Shay, J. L. Burch, R. E. Ergun, B. L. Giles, D. J. Gershman, O. L. Contel, P.-A. Lindqvist, C. T. Russell, R. J. Strangeway, R. B. Torbert, M. R. Argall, D. Fischer, W. Magnes, and L. Franci, Properties of the Turbulence Associated with Electron-only Magnetic Reconnection in Earth’s Magnetosheath, *The Astrophysical Journal* **877**, L37 (2019).
- [13] P. Sharma Pyakurel, M. A. Shay, T. D. Phan, W. H. Matthaeus, J. F. Drake, J. M. TenBarge, C. C. Haggerty, K. G. Klein, P. A. Cassak, T. N. Parashar, M. Swisdak, and A. Chasapis, Transition from ion-coupled to electron-only reconnection: Basic physics and implications for plasma turbulence, *Physics of Plasmas* **26**, 82307 (2019).
- [14] L. V. Kozak, V. A. Pilipenko, O. M. Chugunova, and P. N. Kozak, Statistical analysis of turbulence in the foreshock region and in the Earth’s magnetosheath, *Cosmic*

